ORIGINAL ARTICLE

Journal Section

Induced magnetic states upon electron-hole injection at B and N sites of hexagonal Boron Nitride bilayer: A DFT study

B. Chettri[1,2] | P. K. Patra[1] | Lalmuanchhana[2,3] | Lalhriatzuala[2] | Swati Verma[3] | B. Keshav Rao[3] | Mohan L. Verma[3] | Vishal Thakur[3] | Narender Kumar[3] | Nguyen N. Hieu[4,5] | D. P. Rai[2,*]

[1]Department of Physics, North Eastern Hill University, Shillong , India

[2]Physical Sciences Research Center (PSRC), Department of Physics, Pachhunga University College, Mizoram University, Aizawl-796001, India

[3]Department of Physics, School of Physical Sciences, Mizoram University, Aizawl-796004, India

[4]Department of Applied Physics, FET-SSGI, Shri Shankaracharya Technical Campus, Junwani, Bhilai, Chhattisgarh 490020, India

[5]Institute of Research and Development, Duy Tan University, Da Nang, Viet Nam

[6]Faculty of Natural Sciences, Duy Tan University, Da Nang, Viet Nam

Correspondence
Email: * dibya@pucollege.edu.in

Funding information

We have reported the electronic, magnetic and optical properties of the top layer carbon-doped hexagonal Boron Nitride(h-BN) bilayer at B/N-sites using the density functional theory implemented in Quantumwise VNL-ATK package. The calculated structural and electronic properties of the h-BN bilayer are in agreement with the previously reported results. A single carbon doping on B and N sites modifies the large band gap semiconducting behaviour of h-BN bilayer similar to dilute magnetic semi-conducting material with a net magnetic moment of $1.001\mu_B$ and $0.998\mu_B$, respectively. For double doping at B/N sites net magnetic moment increases to $1.998\mu_B$ and $1.824\mu_B$, respectively. Whereas for triply carbon doped bilayer system at B/N sites, the system changes to metallic behaviour. Upon carbon doping at N-site, we obtained transition from Non-Magnetic semiconductor(Pristine) $\rightarrow$ Magnetic semiconductor(1C) $\rightarrow$ Half-Metal

*Equally contributing authors.

ferromagnetic(2C) → Metal(3C). Whereas, in case of doping at the B-site, we observed transition from Non-Magnetic Semiconductor(Pristine) → Magnetic Semiconductor(1C) → Metal (2C, 3C). Analysis from the PDOS plot of carbon doped systems reveals that the net magnetic moments are contributed by the 2p orbitals of carbon and partial contribution from the neighbouring nitrogen and boron atoms, respectively. As 1,2C doping at the B-site reduces the energy band gap to 0.81-1.8 eV which falls in the visible spectrum and thus such system further opens up an opportunity to be utilised as a photocatalys material. Our carbon doped systems show a magnetic semiconducting behavior with a finite magnetic moment which is one of the criteria for a spintronic material. So, our system looks promising in this regard. Also, Carbon doping can be considered as a simple approach to tune the band gap of the Boron Nitride bilayer system.

KEYWORDS
Spintronics, DFT, B/N-site, Magnetic Moment

1 | INTRODUCTION

Hexagonal Boron Nitride(h-BN) is the lightest Group III-V compound, which shares similar traits to the thinnest and revolutionary 2D material Graphene. Boron Nitride exists in three phases namely hexagonal, cubic and wurtzite. From the experimental and theoretical studies, it's band gap lies in the range of 3.6-6.2 eV [1, 2, 3]. Novoselov et al., using the micromechanical cleavage technique successfully synthesized hexagonal 2D hexagonal Boron Nitride nanosheets [4]. Latter on successful growth of boron nitride crystals was conducted by different techniques[5]. Henceforth, there is a current surge of interest on boron nitride also known as 'White Graphene' due to its common characteristics with graphene [4, 6]. Many other 2D materials such as Transition Metal dichalcogenides, transition metal carbides, graphitic carbon nitride etc., have drawn interest from researchers due to its unique structural, electronic, magnetic and optoelectronic properties [7, 8, 9]. Monolayer and Multilayer structures show interesting phenomena upon twisting, chemical functionalisation, doping, variation of interlayer distance, varying the stacking sequence, applying electric field etc., [10, 11, 12, 13, 14]. Xian et al., on twisting and doping bilayer boron nitride could observe a superconducting behaviour i.e., a transition from a large band gap semiconductor to a superconductor [15]. Xu et al., with the help of a laser with a selected frequency developed a technique to control any stacking sequence further keep it in metastable state [16]. A few layer boron nitride prepared by the dry transfer method shows a superior thermal conductivity as compared to bulk hexagonal boron nitride [17]. In most cases, doping affects the overall profile of the nanostructure materials. Oxygen doping on Boron Nitride bilayer modifies the

interlayer friction properties as revealed by Zhang et al., by performing DFT calculation using Dmol^3 code with GGA-PBE as functional [18]. Flourine doping on bilayer boron nitride results in tuning of band gap, hence enhances its visible light absorption capabilities and shows potential to be utilised in photovoltaic cell applications [19]. Carbon doping on boron nitride lattices was successfully achieved via in situ electron beam irradiation [20]. As boron nitride nanosheets has high refectivity, building a Graphene and hexagonal Boron Nitride multilayer shows metamaterial properties with superior transmission [21]. Experimental evidence of magnetism induced in light element materials with s and p orbitals has been highlighted by Liu et al.,. They synthesized BCN nanosheets by high temperature annealing of stacked BN and graphene nanosheets [22]. Thakur et al., using DFT implemented in SIESTA package studied Graphene and BN hybrid atomic chains and achieved interesting properties such as transition from large band gap semiconductor to metal upon applying strain and electric field [23]. From thorough literature review, we realized that studies on Carbon doped Boron Nitride bilayer has not been performed. So, to explore the effects of carbon doping on the overall profile of the boron nitride bilayer system, we have investigated Carbon doped Boron Nitride bilayer in AA'(Boron(Nitrogen) on top of Nitrogen(Boron)) stacked configuration, which is the most stable one as reported from the density functional theory studies [11, 12, 24, 25].

2 | COMPUTATIONAL DETAIL

We have performed all the calculations using density functional theory(DFT) implemented in Quantumwise VNL-ATK package [26, 27, 28]. The spin polarized meta generalized gradient approximation (SMGGA) with the Strongly Correlated and Appropriately Normed(SCAN) functional was used to describe electronic exchange correlation interaction in all calculations [29, 30]. The sole reason for taking SCAN functional was because of its advantage over the LDA, GGA-PDE and hybridGGA, which fails to describe the van der Waals interactions. SCAN functional fits perfectly for layered system in estimation of its overall profile [30]. A well tested PseudoDojo pseudopotential with medium basis set(similar to double zeta polarized) was used for Boron, Nitrogen and Carbon throughout our calculation [31]. Our supercell was modelled by 3×3×1, which generates 18 atoms in an extended hexagonal sheet of BN in one layer. Whereas, the bilayer now comprises of 18 Boron(B) and 18 Nitrogen(N) atoms and 9 Boron and 9 Nitrogen in each layer. The interlayer spacing is 3.34Å. The cell relaxation was obtained using the Force Field Approximation with Stillinger-Weber potential in a self consistent method with maximum force component on each constituent atom being 0.01 eV/Å. Carbon doping is performed by selectively removing the Boron and Nitrogen atom from its site and substituting it by carbon (C) atom. To create a doping concentration of 0.05%(1C/18(B/N)), 1 atom out of 18 Boron/Nitrogen atoms were removed and similarly removal of 2 and 3 atoms create doping concentration of 0.1%(2C/18(B/N)) and 0.16%(3C/18(B/N)), respectively. The density mesh cut-off was set at 75 Hartree. For structural optimization Brillouin zone integration is performed using 12×12×1 k-point mesh within the Monkhorst-Pack scheme [32]. Whereas,16×16×1 k-point mesh was used for electronic and optical calculations. Calculation of the electron localization function is performed using the function defined by Becke et al. as implemented in Quantumwise VNL-ATK [33]. To check the thermodynamic stability of the doped and undoped bilayer system, we calculated its adhesion energy using the following equation [34] :

$$E_{Ad} = E_{bilayer} - (E_{monolayer-pure} + E_{monolayer-doped}), \quad (1)$$

where $E_{bilayer}$, $E_{monolayer-pure}$ and $E_{monolayer-undoped}$ are the total energies of bilayer, monolayer pure and doped with carbon atom systems, respectively.

3 | RESULTS AND DISCUSSION

3.1 | Structural Properties

We have presented the optimized atomic structure in Fig.1(a-f). The bond length between B-N, B-B, N-N of pristine bilayer system are 1.45, 2.50 and 2.50 Å, respectively. Also the bond angle between B-N-B or N-B-N is 120°. We observed a subtle change in the structural properties in case of carbon doping at B(N) site. In case of 1C doping at B(N) site, N-C(B-C) bond length is 1.48(1.45)Å, respectively. Similar changes in bond length were observed in case of an increase in the C-doping concentration. In case of 2C doping at B(N) site, N-C(B-C) bond lengths are 1.45(1.46) Å, respectively. Upon 3C doping at the B-site, N-C bond length is 1.45Å for nitrogen atom enclosed by 3 carbon and 1.49Å for adjacent N-C bonds. Whereas, B-C and B-N bond length are 1.45Å and 1.44Å when 3C atoms are doped at N-site.

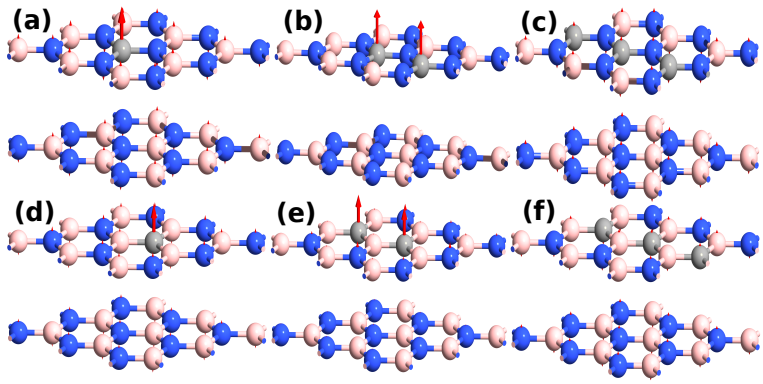

FIGURE 1 . The optimized atomic structure of 1,2,3C doped at B-site(a-c) and 1,2,3C doped at N-site(d-f). Here, Blue→Nitrogen, Brown→Boron, Grey→Carbon. Red arrow on top of B,N and C atoms resembles the induced spin magnetic moment upon doping at B and N sites.

In all cases, B-N bond length remained in between 1.43-1.45 Å. Bond angle at the C-doped hexagonal site varied from 119-120.3°. The atomic structure after C-doping remains planar in all cases. The small variation in the structural parameter(bond-length and bond angle) is due to different atomic radii of the C(dopant), B and N atoms. The interlayer distance for all systems after optimisation is 3.34Å. The structural parameters are in agreement with the previously reported results [25, 35, 36, 37, 38]. To further check the thermodynamic stability of the system, we calculated the adhesion energy from Eqn.1, also presented in Fig.2 (a,b). Negative value of the adhesion energy indicates the stability of bilayer pure(pristine) and doped systems[see Fig. 2(a,b), Table 1].

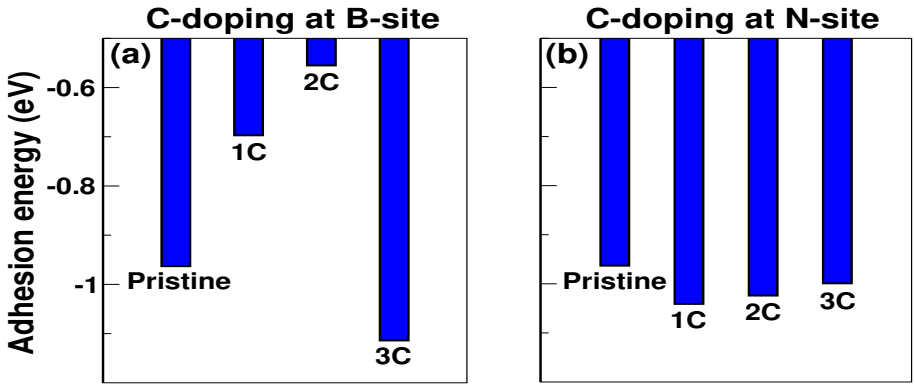

FIGURE 2 Calculated adhesion energies of the C-doped with different concentration at B(a) and N(b)-sites. 1,2,3C represents the number of C-doped at the respective B(N)-sites. Pure system is labelled as pristine.

3.2 | Electronic and magnetic properties

We have presented the electronic band structures of Pristine and the C-doped system at B(N)-site in Fig.3,4(a-d). In Fig.3,4(a-d), $C_{1,2,3}$ resembles the amount of carbon doped at B and N sites. Red and Black lines are for spin-down and spin up band lines. Fig.3(a) for pristine system exhibits a perfect symmetry between spin-up and spin-down channels with an indirect energy band gap of 4.94 eV exhibiting a signature of large band gap non-magnetic semiconductor. The energy band gap obtained for pristine system is consistent and within the range with the earlier reported results [2, 10, 25, 36, 37]. From the calculated Partial Density Of States(PDOS), for pristine system, the top of the valence band is dominated by the N-2p state and the bottom of the conduction band is dominated by the B-2p state with a perfect symmetry between the spin-up and spin-down density of states [see Fig.5(a,e)]. The PDOS represents that the hybridisation around the Fermi-level is due to B,N-2p states. The electronic configuration of Boron, Carbon and Nitrogen are $1s^2 2s^2 2p^1$, $1s^2 2s^2 2p^2$ and $1s^2 2s^2 2p^3$, respectively. Carbon doping at B(N)-site can be considered as electron(hole) injection into the system. So, it is obvious that the doping of C-atom at B(N)-sites will modify the overall properties of the system.

When a B atom is substituted by a C atom, an extra electron is introduced into the structure. As observed from the Fig.3,5(b), doping of $1C_B$(1Carbon at B-site) shifts the whole energy bands from higher energy states to the lower energy states, as a result the energy gap between the Lowest Unoccupied Molecular Orbital(LUMO) and Fermi-level is reduced, and an additional energy level contributed by C-2p orbital is found at the top of the valence band and near to the Fermi-level due to which the energy band gap is reduced. Thus, contribution from the C-2p orbital near the Fermi-level reduces the band gap as well as creates an antisymmetric density of states (DOS) with two values of energy band gaps at the spin-down and spin-up channels exhibiting a behaviour of magnetic semiconductor. The total magnetic moment induced in this system is $1.001\mu_B$ per supercell. The qualitative representation of the induced magnetic moment for all systems is presented in Fig.1. The length of red arrows on the top of the individual atoms gives an idea of strength of the localized magnetic moment. The maximum contribution of the magnetic moment is from the dopant C-atom [see Fig.1(a),5(b)]. The neighbouring B-atoms contributes a partial magnetic moment in the range of 0.018-0.037μ_B. Similarly, in the case of $2C_B$, more impurity states are observed near the Fermi-level

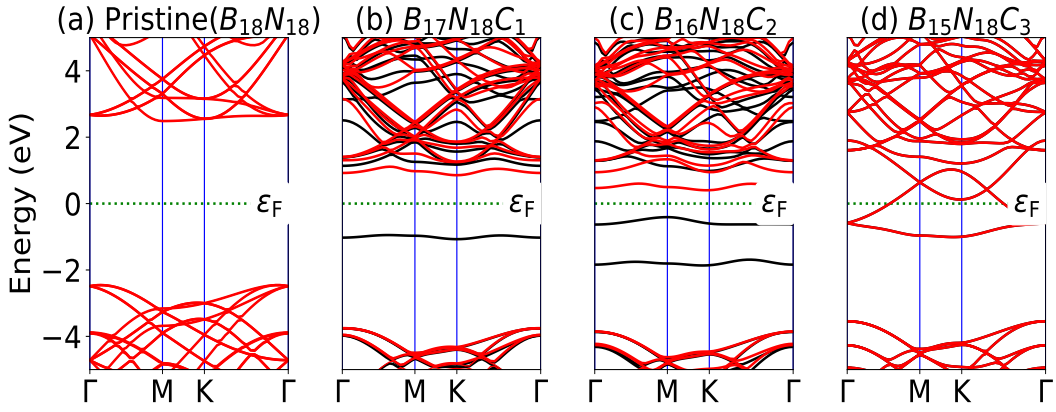

FIGURE 3 . Electronic band structure of (a)Pristine and (b-d)1,2,3Carbon doped system at B-site. Red and black colored lines resembles spin down and spin up band lines respectively.

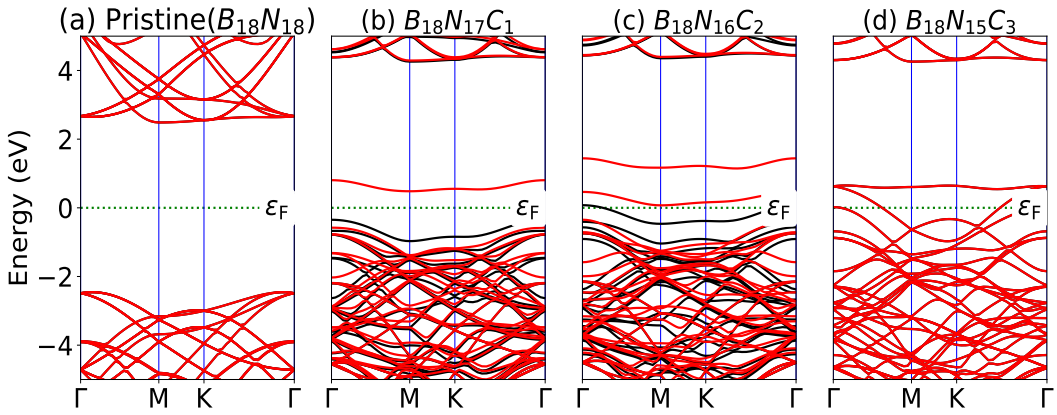

FIGURE 4 . Electronic band structure of Pristine(a) and (b-d)1,2,3Carbon doped system at N-site. Red and black color lines resembles spin-down and spin-up band lines respectively.

thus further reducing the energy band gap to 0.809 eV. The total magnetic moment of the system has increased to 1.998μ_B per supercell. The localized magnetic moment of C-atom atom was found to be 0.813μ_B each. In both cases, the dopant atom has the major contribution and neighbour atom has marginal contribution to the total magnetic moment. Similar observations has been made in case of Carbon doped nanosheets, nanotubes [22, 39, 40]. This observation can be cross verified from the PDOS plot[see Fig.5(b),(c)]. Whereas, in case of $3C_B$, the energy band gap has vanished as the fermi level is populated by the impurity states of C-2p orbitals[see Fig.5(d)]. Also, the system now has magnetic moment of the order of fourth decimal places. Our C-doped system at B-site makes a phase transition from Non-magnetic semiconductor(Pristine) → Magnetic semiconductor(1,2C) → Metal(3C). The calculated total, partial magnetic moment and the energy band gap has been presented in Table1.

Similar to Carbon doping at B-site, we doped C-atom at N-site in the same manner. Doping of Carbon

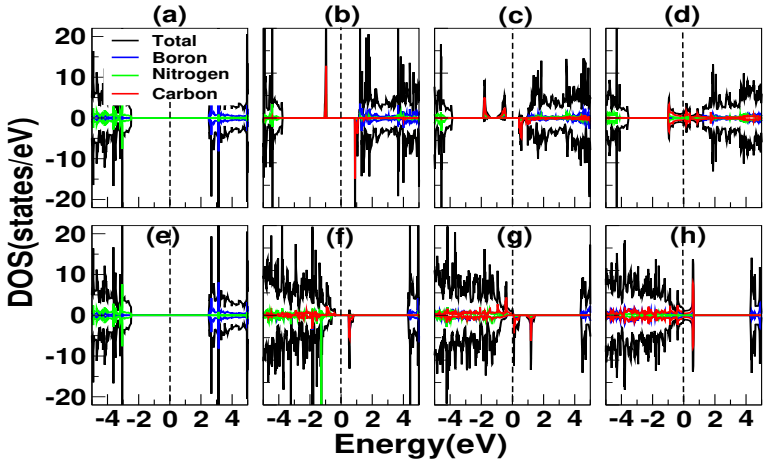

FIGURE 5 Total and Partial density of states(PDOS) is presented here for all the Carbon doped system at B and N sites. (a-d) are for pristine and 1,2,3 carbon doped systems at B-site. Similarly, (e-h) are for pristine and 1,2,3 carbon doped systems at N-site. Here, black, blue, green and red color denotes the total density of states, B-2p, N-2p and C-2p orbitals contribution respectively. Dotted black vertical line at centre represents the fermi-level.

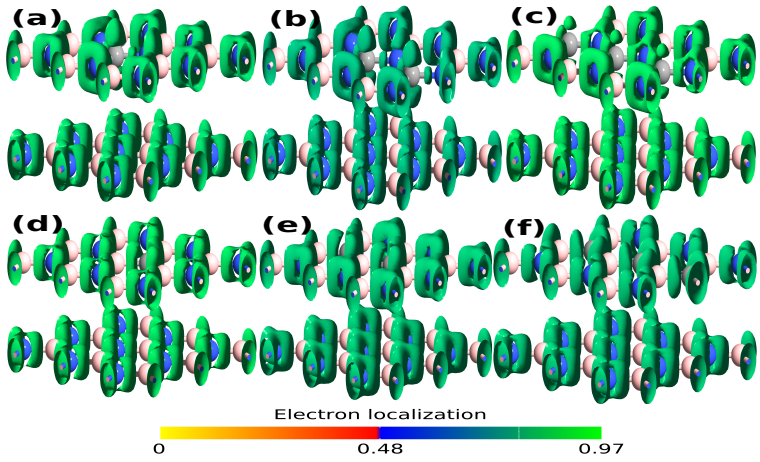

FIGURE 6 (a-c) represents the Electron Localisation Function of the carbon doped system at B site and (d-f) represents the Electron localization function at the N-site. Different colors represents different atoms. Blue-Nitrogen, Brown-Boron and Grey- Carbon.

atom at N-site is similar to injecting a hole into the system, a signature of p-type semiconductor. As observed from the Fig.4(b), substitution of 1N atom by 1C atom moves the entire energy bands to the upper energy levels. The impurity states are introduced near the Fermi level contributed by the C-2p orbital [see Fig.4,5(b),(f)] reducing the energy band gap to 0.830eV. The calculated PDOS shows that the system has now become magnetic due to the antisymmetric spin-up and spin-down states giving a net magnetic moment of $0.998\mu_B$

[see Fig.5(f)]. The contribution of the total and localized magnetic moment is presented in Table1 and can be visualized from the Fig.1. In case of 2C-doping, we can observe a metallic spin-up and semiconducting spin-down channel at the Fermi-level [see Fig.4(g)]. This is a characteristic of a half metal ferromagnet. A net magnetic moment of $1.824\mu_B$ is induced in the system, where majority contribution is from the 2 Carbon dopant atom and marginal contribution from the neighbouring N and B atoms as presented in Table1[22, 39, 40]. A semiconducting system with a net magnetic moment opens up door for developing of spintronic devices. Similar to 3C doped at B-site, 3C doped at N-site shows a metallic behaviour with most impurity states contributed by C-2p orbital at the Fermi level [see Fig.4(h)]. So, our Carbon doped system at N-site makes a phase transition from Non-magnetic semiconductor(Pristine) → Magnetic semiconductor(1C) → Half-Metal Ferromagnet(2C)→ Metal(3C). Thus, the anti-parallel alignment of the magnetic moment of Carbon as well as B and N atoms may be the reason for non-magnetic conducting behaviour of the 3C doped system at B and N sites [20, 40].

TABLE 1 Number of doped carbon, doping site, total and partial magnetic moments, energy band gap(E_g) and adhesion energy(E_{Ad}) is presented below.

No. of C-doped	Doping Site	Total(μ_B)	Partial C (μ_B)	E_{Ad}(eV)	E_g (eV)
0(Pristine)	xxx	xxx	xxx	-0.963	4.94
1	Boron	1.001	0.831	-0.697	1.803
2	Boron	1.998	0.813	-0.555	0.809
			0.813		
3	Boron	0.000	xxx	-1.114	0.00
1	Nitrogen	0.998	0.665	-1.041	0.830
2	Nitrogen	1.824	0.606	-1.024	0.00
			0.606		
3	Nitrogen	0.000	xxx	-0.999	0.00

To have a better understanding of the bonding characteristics in pristine and carbon doped Boron Nitride bilayer, we have presented an Electron Localisation Function and Electron density distribution plots in Fig.6,7(a-f). The value of Electron Localisation Function lies between 0 to 1. The isovalue for electron density is taken as $1.95 Å^{-3}$. Information about the localized electrons can be obtained by visualising the region where the ELF value is high. Green lobe in the ELF distribution plot gives the idea of bonding characteristics and electron distribution. For 1C(Grey in color) doped at B-site, the majority of electrons are localized around the nitrogen(ionic) atom and small fraction of electron localization is observed between Carbon and Nitrogen atom(covalent) at the doping site. Some fraction of electron are localised around Carbon atom too [see Fig.6(a)]. A similar trend is followed in 2C and 3C doped systems at B-site. In case of 1,2,3-Carbon doped at N-site, we can see small electron localization closer to C atom(similar to Nitrogen atom but less in quantity) and partially shared between the neighbor Boron atoms resembling admixture of ionic and covalent bond. The nature of chemical bond between B-N atoms away from the doping site are of partially ionic and

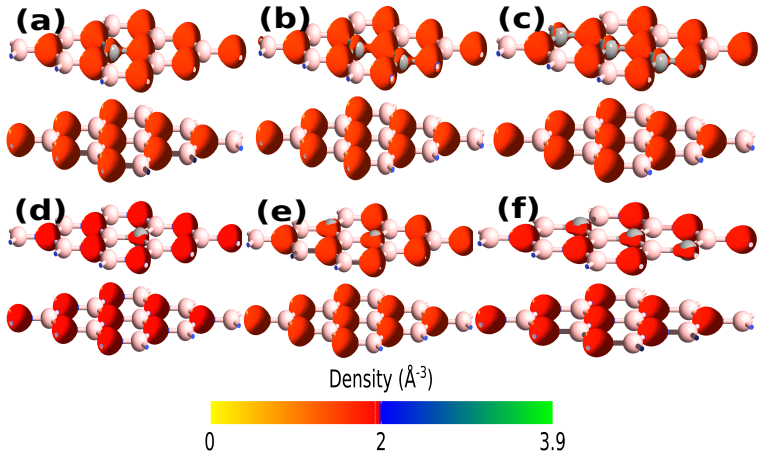

FIGURE 7 Electron density distribution plot is presented here. (a-c) are for 1,2,3Carbon doped at B-site and (d-f) are for 1,2,3Carbon doped at N-site.

covalent as evident from the electron localization close to N-atom. Also, this observations is cross-verified from the electron density plot, where most charge density is around Nitrogen and feeble around Carbon atom [see Fig.7(a-f)]. Thus, we can conclude that the bonding characteristics between B-N, N-C and B-C are a mixture of ionic and covalent bonds upon C-doping at B/N sites [see Fig.6(a-c),6(d-f)][36, 41, 42, 43].

3.3 | Optical Properties

Optical properties such as dielectric function and absorption coefficients with respect to the photon energy are presented in this section for the pristine and bilayer boron nitride system doped with 1,2,3C at B/N-sites. The theoretical part for calculating the optical properties has been well explained by Marinopoulos et al., [44]. The real part and imainary part of dielectric function can be expressed as,

$$\epsilon = \epsilon_1 + \iota\epsilon_2, \tag{2}$$

Here ϵ_1 and ϵ_2 are real and imaginary parts of the dielectric function respectively. The imaginary part can be calculated using Eqn.(2),

$$\epsilon_2(\omega) = \frac{\hbar^2 e^2}{\pi m^2 \omega^2} \Sigma_{nn'} \int_k d^3k | < \overrightarrow{k}\, n | \overrightarrow{p} | \overrightarrow{k}\, n' > |^2 [1 - f(\overrightarrow{k}\, n)] \delta(E_{\overrightarrow{k}\, n} - E_{\overrightarrow{k}\, n'} - \hbar\omega), \tag{3}$$

where $\overrightarrow{p}$ - momentum operator, $|\overrightarrow{k}\, n >$ - eigenfunction of eigenvalue, f($\overrightarrow{k}\, n$)- Fermi Distribution function. The Kramers-Kronig transformation helps in finding the real part of the dielectric function from its corresponding imaginary part as :

$$\epsilon_2(\omega) = 1 + \frac{2}{\pi} \int_0^\infty \frac{\epsilon_2(\omega')\omega' d\omega'}{\omega'^2 - \omega^2}, \tag{4}$$

The absorption coefficients $\alpha(\omega)$, which is related to the dielectric function is given as follows;

$$\alpha(\omega) = \frac{2\omega(|\epsilon(\omega)| - Re\epsilon(\omega))^{1/2}}{c} \tag{5}$$

We have used black, red, green and blue color in all the latter figures to represent the pristine, 1,2 and $3C_{B/N}$ carbon doped at B(N) site bilayer systems. The absorption coefficient for the pristine and carbon doped boron nitrtide bilayer at B-site has been presented in Fig.8. For pristine bilayer system along X-axis a single peak is observed at photon energy 5.8eV with an absorption coefficient of $3.5 \times 10^5 \text{cm}^{-1}$ and has zero adsorption in the photon energy range 0-4eV and beyond 7.8eV[see Fig.8(a)]. Whereas, in case of out of plane symmetry i.e., along Z-axis double peak at energy 5.4eV and 5.8eV are observed with absorption coefficient $2.1 \times 10^4 \text{cm}^{-1}$ and $2.25 \times 10^4 \text{cm}^{-1}$, respectively and zero adsorption remains same as in the case of in the plane symmetry(along X-axis) [see Fig.8(b)]. The findings are well in agreement with the earlier reported results [36, 45]. When one carbon($1C_B$) is doped at B-site, two peaks are observed at energy

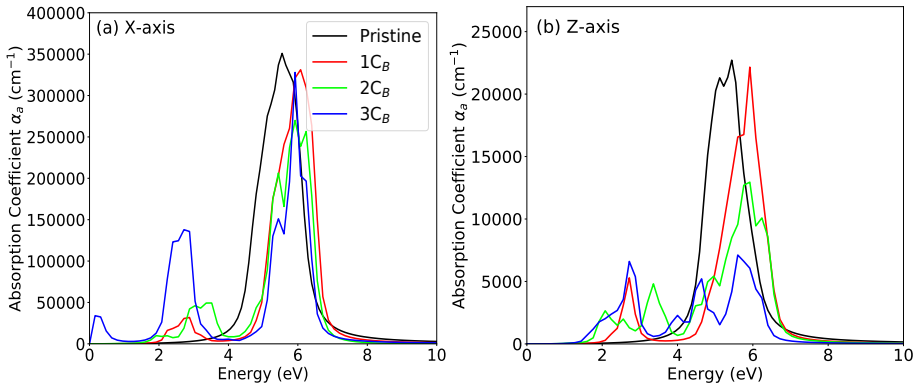

FIGURE 8 Absorption coefficient of the Pristine and 1,2,3Carbon doped system at the B-site. In above figures, (a) is for in plane symmetry i.e., along X-axis whereas (b) is for out of plane symmetry i.e., along Z-axis. Here, 1,2,3C_B denotes the number of carbon doped at N-site. Doping concentration are individually labelled and presented with respective colors.

2.8eV(small) and 6.2eV(large) respectively. There is a little shift in the absorption peak toward higher energy. Similarly, in the case of two and three carbon doped at B-site(2,3C_B) large absorption peak lies in 6.0-6.2eV with small absorption peak at a lower energy range. So, carbon doping at B-site shifts the main absorption peak toward higher energies, which corresponds to blue shift [46]. The absorption coefficient intensity for large peaks in case of pristine and 1,2,3C_B system along X and Z lies in the range $2.75 - 3.5 \times 10^5 \text{cm}^{-1}$ and $0.6 - 2,25 \times 10^4 \text{cm}^{-1}$ respectively [see Fig.8(a,b)]. The additional small peaks in 1,2,3C_B-doped system, have been attributed to the C-2p impurity states near the fermi level as observed from the density of states and band structure [see Fig.3(b),5(b)]. The peaks that has been observed in Carbon doped system is because of the transition between B, N, C-2p states. Zero absorption is observed beyond 7.0eV for 1,2,3C_B-doped system. The real(a,c) and imaginary(b,d) part of the dielectric function for pristine and carbon doped bilayer at B-site(1,2,3C_B) has been presented in Fig.9. The static dielectric function of the pristine and carbon doped bilayer system in plane(along X) and out of plane(along Z) symmetry are 1.271, 1.221, 1.223, 27.62 and 1.014, 1.013, 1.016, 1.020, respectively. An interesting observation can be made from Fig.9(a), that at

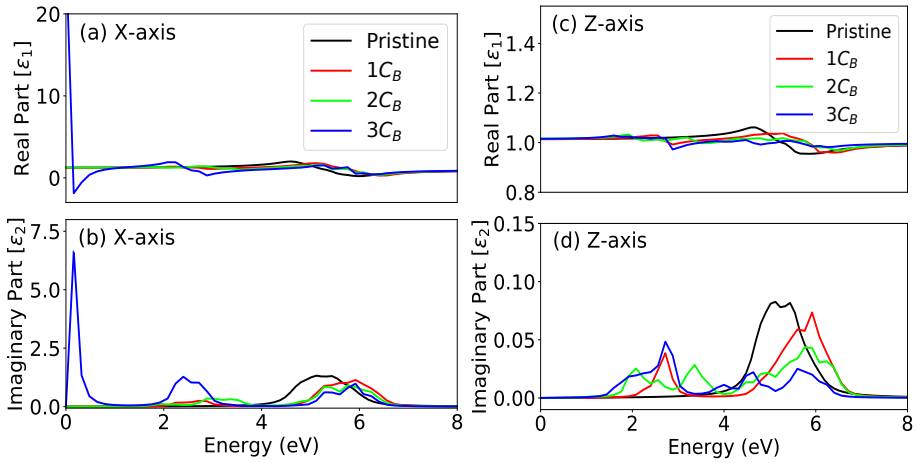

FIGURE 9 The (a,c)real and (b,d)imaginary part of the dielectric function for Pristine and 1,2,3C_B doped at B-site which are measured along X- and Z-axes are presented here. In above figures, (a,b) are for in plane symmetry i.e., along X-axis whereas (c,d) are for out of plane symmetry i.e., along Z-axis. Here, 1,2,3C_B denotes the number of carbon doped at B-site. Doping concentration are individually labelled and presented with respective colors

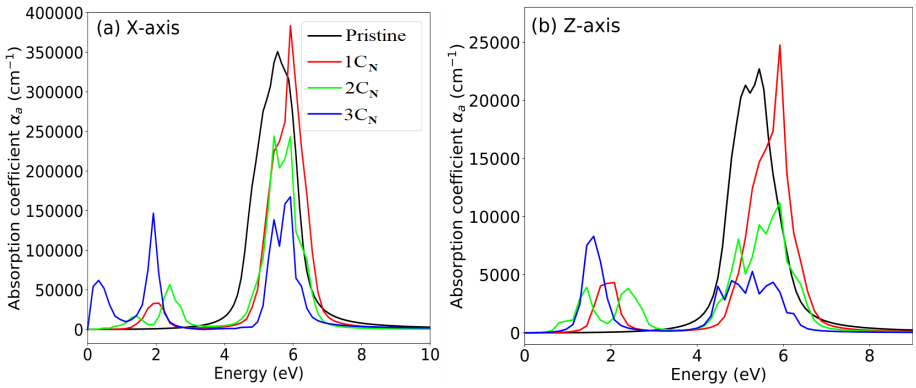

FIGURE 10 Absorption coefficient of the Pristine and 1,2,3 Carbon doped system at the N-siteS. In above figures, (a) is for in plane symmetry i.e., along X-axis whereas (b) is for out of plane symmetry i.e., along Z-axis. Here, 1,2,3-C_N denotes the number of carbon doped at N-site. Doping concentration are individually labelled and presented with respective colors

energy range 0.18-0.36 eV, the static dielectric constant for 3C_B system becomes negative which is an intrinsic property of metamaterials(negative index materials) [47] and similar observation was made in case of vacancy defects in h-BN bilayer system at B and N site [36, 45]. In recent studies, Graphene-Hexagonal boron nitride multilayer has shown negative index properties [21]. It is because of plasmonic vibration created due to the intraband transitions. Whereas, the real part of the dielectric constant remains positive for all systems along Z-axis. The imaginary part of the dielectric function is correlated with the absorption coefficient, as seen from Fig.8(a,b),9(b,d).

The optical response in terms of absorption coefficient and the dielectric function of the carbon doped bilayer

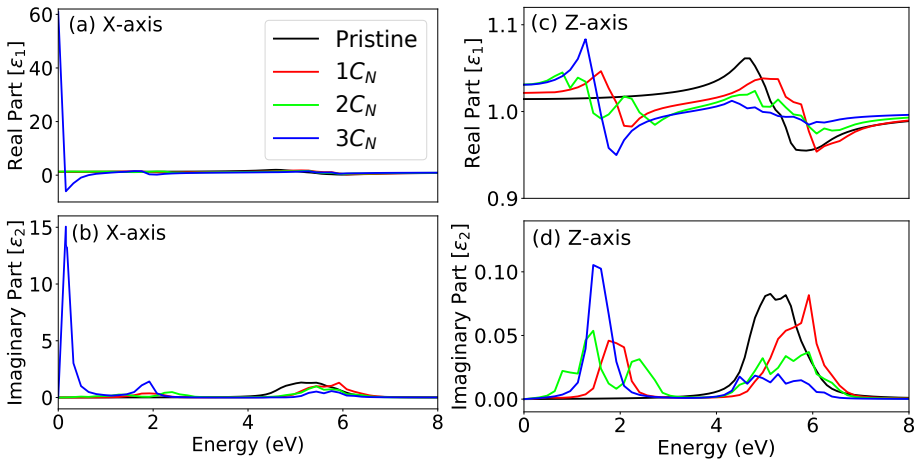

FIGURE 11 The (a,c)real and (b,d)the imaginary part of the dielectric function for Pristine and 1,2,3C$_N$ doped at N-site which are measured along X- and Z-axes are presented here. In above figures, (a,b) are for in plane symmetry i.e., along X-axis whereas (c,d) are for out of plane symmetry i.e., along Z-axis. Here, 1,2,3C$_N$ denotes the number of carbon doped at N-site. Doping concentration are individually labelled and presented with respective colors

system at N-site(1,2,3C$_N$) in plane(along X) and out of plane(along Z) symmetry are presented in Fig.10(a,b) and Fig.11(a-d), respectively. In case of (1,2,3C$_N$) systems, the absorption peak has shifted to higher energy range resembling a blue shift for both the in plane and out of plane symmetry. Larger absorption peak are observed at energies 6.2eV, 6.1eV and 6.1eV for (1,2,3C$_N$) along X-axis, respectively. Few smaller absorption peaks(0.4-3.0eV and) are also present due to the transition between the induced defect states near the Fermi-level due to carbon doping and B and N-2p states along X, Z-axis [see Fig.10(a,b)]. In Fig.11(a-d), real and imaginary part of the dielectric function for 1,2,3C$_N$ doped at N-site along X and Z-axis is presented. The static dielectric constants for 1,2,3C$_N$ doped at N-site along X and Z-axis are are 1.221, 1.351, 61.056 and 1.018, 1.030, 1.051, respectively. Similar to 3C$_B$ system, the real part of the dielectric constant attains negative value at energy range 0.22-0.0.50 eV for 3C$_B$ doped system along X-axis.

4 | CONCLUSION

A DFT calculation was performed to investigate the effect of carbon doping at B and N-sites on the structural, electronic, magnetic and optical properties of the AA' stacked boron nitride bilayer system. We showed that the C-doping at B and N site is feasible and the structure remains stable as evident from the negative adhesion energy value. Upon C-doping there is negligible change in bond length and bond angle. The structural parameters are well in good agreement with the previous results. The increase in doping concentration at B-site(electron injection) induces a phase transition from Non-Magnetic Semiconductor (Pristine) → Magnetic Semiconductor(1C,2C) → Metal(3C). Similarly, doping at N-site(hole injection) induces a phase transition from Non-Magnetic Semiconductor(Pristine) → Magnetic Semiconductor(1C) → Half-Metal(2C) →

Metal(3C). The total magnetic moment for 1,2C doped at B(N)-site are 1.001(0.998), 1.998(1.824) μ_B respectively. In summary, carbon doping at B and N sites favors spin polarization and created partial magnetic moments. Negative real part of the dielectric function is a property of metamaterials and our system have such characteristics in some particular energy range. Electron and hole injection into a bilayer boron nitride system reveals interesting properties and can be further used in building nanoelectronic devices.

Acknowledgements

D. P. Rai acknowledges Core Research Grant from Department of Science and Technology SERB (CRG DST-SERB, New Delhi India) via File no.CRG/2018/000009(Ver-1).

references

[1] Y. Lin, J. W. Connell, Advances in 2D Boron Nitride Nanostructures: nanosheets, nanoribbons, nanomeshes and hybrids with graphene. Nanoscale 4(22) (2012) 6908. https://doi.org/10.1088/0957-4484/22/21/215603.

[2] J. Olander, K. Larsson, Initial growth of hexagonal and cubic boron nitride:A theoretical study. Phys. Rev. B 68 (7) (2003) 075411. https://doi.org/10.1103/PhysRevB.68.075411.

[3] M. Topsakal, E. Akturk, S. Ciraci, First-principles study of two- and one-dimensional honeycomb structures of boron nitride. Phys. Rev. B 79 (2009) 115442. https://doi.org/10.1103/PhysRevB.79.115442.

[4] K. S. Novoselov, D. Jiang, F. Schedin, T. J. Booth, V. V. Khotkevich, S. V. Morozov, A. K. Geim, Two-dimensional atomic crystals. Proc. Natl. Acad. Sci. 102 (2005) 10451-10453. https://doi.org/10.1073/pnas.0502848102.

[5] L. X. Lin, Z. H. Li, Y. Zheng, A. S. Ahmed, Size-dependent oriented attachment in the growth of pure and defect-free hexagonal boron nitride nanocrystals. Nanotechnology 22 (2011) 215603. https://doi.org/10.1088/0957-4484/22/21/215603.

[6] K. S. Novoselov, A. K. Geim, S. V. Morozov, D. Jiang, Y. Zhang, S. V. Dubonos, I. V. Grigorieva, A. A. Firsov, Electric Field Effect in Atomically Thin Carbon Films. Science 306 (2004) 666-669. https://doi.org/10.1126/science.1102896.

[7] D. P. Rai, T. V. Vu, A. Laref, M.P. Ghimire, P.K. Patra, S. Srivastava, Electronic and optical properties of 2D monolayer (ML) MoS2 with vacancy defect at S sites. Nano-Structures and Nano-Objects 21 (2020) 100404. https://doi.org/10.1016/j.nanoso.2019.100404.

[8] A. Laref, M. Alsagri, S. M. Alay-e-Abbas, S. Laref, H. M. Huang, Y. C. Xiong, J. T. Yang, S. A. Khandy, D. P. Rai, D. Varshney, X. Wu, Electronic structure and optical characteristics of AA stacked bilayer graphene: A first principles calculations. Optik (2019) 163755. https://doi.org/10.1016/j.ijleo.2019.163755.

[9] K. O. Obodo, C. N. M. Ouma, J. T. Obodo, M. Braun, D. Bessarabov, First principles study of single and multi-site transition metal dopant ions in MoS2 monolayer. Computational Condensed Matter 21 (2019) e00419. https://doi.org/10.1016/j.cocom.2019.e00419.

[10] Y. Fujimoto, S. Saito, Interlayer distances and band gap tuning of hexagonal Boron-Nitride bilayers. Journal of Ceramic Society of Japan.124(5) (2016) 584-586.

[11] S. M. Gilbert, T. Pham, M. Dogan, S. Oh, B. Shevitski, G. Schumm, S. Liu, P. Ercius, S. Aloni, M. L. Cohen, A. Zettl, Alternative stacking sequences in Hexagonal Boron Nitride. 2D Mater. 6 (2018) 021006. https://doi.org/10.1088/2053-1583/ab0e24

[12] N. Marom, J. Bernstein, J. Garel, A. Tkatchenko, E. Joselevich, L. Kronik, O. Hod, Stacking and Registry Effects in Layered Materials: The Case of Hexagonal Boron Nitride. PRL 105 (2010) 046801.

[13] Lalrinkima, Lahriatzuala, D. P. Rai, S. Srivastava, Strain dependence of electronic properties and effective masses of monolayer ZnO from density functional theory. AIP Conference Proceedings 2115 (2019) 030093. https://doi.org/10.1063/1.5112932.

[14] D. P. Rai, T. V. Vu, A. Laref, H.Joshi, P. K. Patra, Promising optoelectronic response of 2D monolayer MoS2: A first principles study. Chemical Physics 538 (2020) 30093. https://doi.org/10.1016/j.chemphys.2020.110824.

[15] L. Xian, D. M. Kennes, N. T. Dejean, M. Altarelli, A. Rubio, Multiflat bands and strong correlations in Twisted Bilayer Boron Nitride: Doping-Induced correlated insulator and superconductor. Nano Lett. 119 (2019) 4934-4940.

[16] H. Xu, J. Zhou, Y. Li, R. Jaramillo, J. Li, Optomechanical control of stacking patterns of h-BN bilayer. Nano Res., 12 (2019) 2634 —2639. 10.1016/j.physrep.2016.07.003.

[17] C. Wang , J. Guo , L. Dong , A. Aiyiti , X. Xu and B. Li, Superior thermal conductivity in suspended bilayer hexagonal boron nitride. Sci. Rep. 6 (2016) 25334. 10.1038/srep25334.

[18] J. Zhang, L. An, B. Zhang, J. Zhang, Y. Yu, C. Wang, Interlayer friction properties of oxygen-doped hexagonal boron nitride bilayers. EPL 127 (2019) 16003. 10.1209/0295-5075/127/16003.

[19] J. Zhang, B Zhang, Y. Yu, C-M. Wang, First-principles insights of electronic and optical properties of F-doped hexagonal boron nitride nanosheets for photo-catalytic water splitting. EPL 127 (2019) 67003. 10.1209/0295-5075/127/67003.

[20] X. Wei, M. Wang, Y. Bando, D. Golberg, Electron-Beam-Induced Substitutional Carbon Doping of Boron Nitride Nanosheets, Nanoribbons, and Nanotubes. ACS Nano 5(4) (2011) 2916–2922. 10.1021/nn103548r.

[21] A. A. Sayem et al., Negative Refraction with Superior Transmission in Graphene-Hexagonal Boron Nitride (hBN) Multilayer Hyper Crystal. Sci. Rep. 6 (2001) 25442. 10.1038/srep25442.

[22] W. Liu, T Yanase, T. Nagahama, T. Shimada, Synthesis of carbon-doped boron nitride nanosheets and enhancement of their room-temperature ferromagnetic properties. Journal of Alloys and Compounds 792 (2019) 1206-1212. https://doi.org/10.1016/j.jallcom.2019.04.136.

[23] V. Thakur, N. Kumar, M. L. Verma, A. Kumar Choubey, S. Verma, B. Chettri, H. D. Sahu, B. K. Rao, Density functional study on hybrid h-BN/graphene atomic chains. Physica E: Low-dimensional Systems and Nanostructures 124 (2020) 114316. https://doi.org/10.1016/j.physe.2020.114316.

[24] A. V. Lebedev, I. V. Lebedeva, A. A. Knizhnikac, A. M. Popov, Interlayer interaction and related properties of bilayer hexagonal boron nitride: ab initio study. Phys. Rev. B 93 (2016) 235414. https://doi.org/10.1039/C6RA90034H.

[25] G. Constantinescu, A. Kuc, T. Heine, The Stacking in Bulk and Bilayer Hexagonal Boron Nitride Phys. Rev. Lett. 111 (2013) 036104 .

[26] W. Kohn, L. J. Sham, Self-Consistent Equations Including Exchange and Correlation Effects. Phys. Rev. 140(4A) (1965) A1138-A1133. https://doi.org/10.1103/PhysRev.140.A1133

[27] ATOMISTISTIX TOOLKIT version 2018.06, QuantumWise A/S. www.quantumwise.com.

[28] S. Smidstrup et al. QuantumATK: an integrated platform of electronic and atomic-scale modelling tools. J. Phys.: Condens. Matter 32 (2020) 015901. https://doi.org/10.1088/1361-648X/ab4007.

[29] J. M. Del Campo, J. L. Gazquez, S. B. Trickey, A. A. Vela, A new meta-GGA exchange functional based on an improved constraint-based GGA. Chem. Phys. Lett. 543 (2012) 179–183 . https://doi.org/10.1016/j.cplett.2012.06.025

[30] J. Sun, R. Remsing, Y. Zhang et al., Accurate first-principles structures and energies of diversely bonded systems from an efficient density functional. Nature Chem. 8 (2016) 831–836. https://doi.org/10.1038/nchem.2535.

[31] S. Smidstrup et al., First principles Green's function method for surface calculations: A pseudopotential localized basis set approach Phys. Rev. B 96 (2017) 195309. https://doi.org/10.1103/PhysRevB.96.195309.

[32] H. J. Monkhorst, J. D. Pack, Special points for brillouin zone integrations. Phys. Rev. B 13 (1976) 5192-5188 .DOI:https://doi.org/10.1103/PhysRevB.13.5188.

[33] A. D. Becke, K. E. Edgecombe. A simple measure of electron localization in atomic and molecular systems. J. Chem. Phys., 92 (1990) 5397. https://doi.org/10.1063/1.458517.

[34] M. R. A. Kishore, K. Larsson, P. Ravindran, Two-Dimensional CdX/C2N(X = S,Se) Heterostructures as potential Photocatalysts for Water Splitting: A DFT Study. ACS Omega,5 (2020) 23762-23768. https://dx.doi.org/10.1021/acsomega.0c02804.

[35] O. Hod, Graphite and hexagonal Boron-Nitride have the same interlayer distance.Why? J. Chem. Theory Comput. 8(4) (2012) 1360-1369. DOI: 10.1021/ct200880m

[36] B. Chettri et al. Induced ferromagnetism in bilayer hexagonal Boron Nitride (h-BN) on vacancy defects at B and N sites. Physica E: Low-dimensional Systems and Nanostructures 126 (2021) 114436. https://doi.org/10.1016/j.physe.2020.114436.

[37] F. Hummel, T. Gruber , A. Grüneis, A many-electron perturbation theory study of the hexagonal boron nitride bilayer system Eur. Phys. J. B 89 (2016) 235. https://doi.org/10.1140/epjb/e2016-70177-4.

[38] J. Ryou, J. Park, S. Hong, Investigations of Vacancy Structures Related to Their Growth in h-BN Sheet. Nanoscale Res. Lett. 12 (2017) 445. https://doi.org/10.1186/s11671-017-2194-6.

[39] R. Q. Wu, L. Liu, G. W. Peng, Y. P. Feng, Magnetism in BN nanotubes induced by carbon doping. Appl. Phys. Lett. 86 (2005) 122510. http://dx.doi.org/10.1063/1.1890477.

[40] C. Zhao, Z. Xu, H. Wang, J. Wei, W. Wang, X. Bai, E. Wang, Carbon-Doped Boron Nitride Nanosheets with Ferromagnetism above Room Temperature. Adv. Funct. Mater. 24 (2014) 5985–5992. 10.1002/adfm.201401149.

[41] Y. Lin, J. W. Connell. Advances in 2D Boron Nitride Nanostructures: Nanosheets, Nanoribbons, Nanomeshes, and Hybrids with Graphene. Nanoscale 4(22) (2012) 6908. DOI: 10.1039/c2nr32201c.

[42] G. Mierzwa, A. J. Gordon, S. Berski, The nature of multiple boron-nitrogen bonds studied using electron localization function (ELF), electron density (AIM), and natural bond orbital (NBO) methods. J. Mol. Model 26 (2020) 136. https://doi.org/10.1007/s00894-020-04374-9.

[43] A. D. Becke and K. E. Edgecombe. A simple measure of electron localization in atomic and molecular systems. J. Chem. Phys.,92 (1990) 5397. https://doi.org/10.1063/1.458517.

[44] A. Marinopoulos, L. Reining, A. Rubio, V. Olevano, Ab initio study of the optical absorption and wave-vector-dependent dielectric response of graphite. Condens. Matter Phys. 69 (2004) 245419 . http://dx.doi.org/10.1103/PhysRevB.69.245419.

[45] K. A. Mengle, E. Kioupakis, Impact of the stacking sequence on the bandgap and luminescence properties of bulk, bilayer, and monolayer hexagonal boron Nitride. APL Mater. 7 (2019) 021106. DOI:10.1063/1.5087836

[46] M. Goudarzi, S. S. Parhizgar, J. Beheshtian, Electronic and optical properties of vacancy and B, N, O and F doped graphene: DFT study. Opto-Electronics Review 27 (2019) 130-136 . http://doi.org/10.1016/j.opelre.2019.05.002.

[47] R. A. Shelby, D.R. Smith, S. Shultz, S.C. Nemat-Nasser, Microwave transmission through a two-dimensional, isotropic, left-handed metamaterial. Applied Physics Letters 78(4) (2001) 489 . http://doi.org/10.1063/1.1343489.